Reversible and reusable compartmentalized microfluidic chip for coculture of dorsal root ganglion neurons

Solène Moreau, Raul Flores-Berdines, Anne Simon, Tatiana El Jalkh, Guillaume Taret, Anna Fomina, Céline Dargenet-Becker, André Estevez-Torres, Sophie Bernard and Hugo Salmon**

* Contributed equally

E-mail: sophie.bernard@u-paris.fr; hugo.salmon@u-paris.fr

S. Moreau, C. Dargenet-Becker, A. Simon, A. Fomina, G. Taret, S. Bernard, H. Salmon
Université Paris Cité, Inserm, HEALTHFEX, 45, rue des Saints Pères 75006 Paris, France

R. Flores-Berdines, H. Salmon
Université Paris Cité, CNRS, Inserm, NABI, 45, rue des Saints Pères 75006 Paris, France

T. El Jalkh
IMRB INSERM U955 Université Paris-Est
51, avenue du Maréchal de Lattre de Tassigny 94010 Créteil, France

A. Estevez-Torres
LASIRE UMR CNRS 8516 Université de Lille
Avenue Paul Langevin 59650 Villeneuve-d'Ascq, France

Abstract

Compartmentalized microfluidic chips play an important role in understanding the cellular mechanisms involved in neurodegenerative disorders. Dorsal root ganglia are a well-established model for modelling the peripheral nervous system (PNS), but their development on a chip remains limited. Furthermore, it would be beneficial for the devices to be openable in order to access the biological material inside for analyses. Easy to prototype and biocompatible, styrenic block copolymers (SBC) are an alternative to polydimethylsiloxane (PDMS) that offer both reversible and permanent bonding properties. This paper presents a fast and straightforward method to produce compartmentalized SBC chips. The study validates the culture of murine dorsal root ganglia explants, comparing it to the standard methods, to obtain a model of the PNS. Moreover, the reversible bonding properties of the SBC permit the reuse of the chip with a quick and easy cleaning protocol. It provides direct access to the cells, opening the way for imaging and molecular biology analysis. The comparison of the resources required to produce PDMS and SBC chips highlights the importance of moving to reusable devices. These detachable, easy-to-manufacture and sustainable all-thermoplastic platforms provide an alternative way of prototyping compartmentalized devices *for in vitro* PNS modeling.

Keywords: Microfluidic chip, Dorsal root ganglia, sensory neurons, compartmentalized culture, styrenic bloc copolymers, soft thermoplastic elastomers

1. Introduction

The reduction of animal numbers and their replacement by alternative experimental methods are two of the 4R principles (reduction, replacement, refinement, and responsibility) and constitute a major strategic ethical challenge, prompting the development of *in vitro* models that can be used instead of *in vivo* studies involving animal models. In neuropharmacology, where time scales and the complexity of the physiology are particularly high, the development of structurally and functionally pertinent potency tests that are easily accessible remains a major challenge to accelerate the translation of therapeutics.[1] In particular, when these alternative models can be used as screening platforms to evaluate drug candidates through rapid and simple monitoring of the physiological response of the nervous system to drugs.

Microfluidic devices for compartmentalized culture have offered the possibility to study the neuronal functions and structures in a highly controlled way.[2,3] Robert Campenot was the first to develop a device that enabled local control of axons and somas.[4] The aim was to physically separate the cell bodies from the axons to mimic the diverse microenvironments that a neuron might encounter. Subsequently, a variety of microfluidic devices have been developed for neuronal studies. Taylor initiated a two-compartment microfluidic device connected by straight microchannels [5] for the study of axonal injury, regeneration and transport. Samson *et al.* employed a five-parallel culture chamber configuration to circumvent cross-contamination and to establish an environmentally isolated neuronal population with synaptically interconnected cells.[6] Courte *et al*. designed a microchip with arc-shaped microchannels to control the orientation and filtering of axonal growth.[7] Sharma *et al.* proposed a keyhole design to model human nerves [8], while Park *et al.* developed central circular chamber designs to promote axon growth in microchannels and the formation of a denser axonal network layer [9,10]. Electrospun aligned nanofiber-integrated compartmentalized microfluidic neuron culture systems have been developed by Luo *et al.* to improve axon alignment, length and stability. [11]Two-dimensional (2D) and three-dimensional (3D) compartmentalized co-culture systems on microdevices have been developed to analyze the interactions between neurons and glial cells in both the central nervous system (CNS) [10,12] and in the peripheral nervous system (PNS).[8,10,13–15]

Most of the PNS models focus on motor neurons, while there are only a few studies on sensory neurons on chip.[16–19] However, these studies focus on co-cultures of sensory neurons and oligodendrocytes, a glial cell that is specific to the central nervous system. Dorsal root ganglia (DRGs) represent a well-established model for PNS modeling, but their development on a chip remains limited. They mainly focus on pain signaling[20] and therapeutics[21] as well as on "nerve-on-chip"[22,23]. In 2023, Mutschler *et al*. [24] proposed the first co-culture of neurons from dissociated DRGs and Schwann cells on a compartmentalized microfluidic device. They highlighted the challenge of culturing DRGs as explants in microfluidic chips. Notably, Park *et al.* were the only group to successfully culture a chick DRG

explant in a compartmentalized microfluidic device.[25] To facilitate the seeding of the explant, they designed a device with an open-top chamber.

Compartmentalized systems and organ-on-chip devices are becoming more widespread in the field of Biology, prompting a re-evaluation of their sustainability and of the materials used in their manufacture for specific applications.. Currently, polydimethylsiloxane (PDMS) is predominantly used due to its high oxygen permeability, while polystyrene (PS) is favored for large-scale production and alignment with biological standards.[26] However, there are no neurobiological applications that utilise materials combining the advantages of PDMS and PS, such as styrenic block copolymers (SBCs).[27] Reversible bonding of SBCs would be an advantage for accessing tissues during culture and for reusing devices .[28–30] Moreover, as the organ-on-chip industry is expanding rapidly and access and production costs are becoming critical for laboratory resources and carbon footprint,[31] there is no known comprehensive assessment or methodology to evaluate the resources involved. Here, we describe a fast and straightforward method for the fabrication of compartmentalized SBC chips and demonstrate their reversible bonding and reusability for the culture of compartmentalized peripheral nervous system model. We first propose a simple process for fabricating SBC chips with an axisymmetric design adapted to anisotropic compartmentalized culture, particularly suitable for primary DRG explants. We confirm the theoretical compatibility of the design with neuron culture using analytical and finite element models. The viability and axonal growth of E13.5 mouse embryonic DRGs within SBC and equivalent PDMS chips were then compared. We present a rapid and reliable cleaning procedure for SBC chips and evaluate their reusability. We also demonstrate the potential of reversible bonding chips for direct imaging using electron microscopy, as well as for biological analysis techniques (immunostaining, Western blot, RT-qPCR). Finally, we discuss the resources (energy, time, cost and CO_2 equivalent emission) involved in the production of a PDMS compared to an SBC chip.

2. Results

2.1. Development of a compartmentalized SBC chip for coculture of DRG neurons

With the exception of the photolithography step, which is necessary for $10\ \mu m$ wide channels, the fabrication process of SBC microfluidic chips **(Figure 1A)** is an out-of-the-cleanroom process. The first phase was to replicate the SU-8 mold in an epoxy one to obtain a mold more suitable for hot embossing. The replication of the molds was confirmed by profilometry *(***Figure SI.1***)*. Once this step has been achieved, the epoxy mold can be used as many times as required to emboss SBC devices. Our epoxy molds have been in use for 2 years, have embossed more than 200 chips without damage and are still in use. They are embossing at 0.7 MPa and 160°C for 3 min. This temperature is higher than the melting temperature (120°C) of the soft thermoplastic elastomer (sTPE) to reach its viscoelastic

state.[30] Fabrication of the SBC chip takes around 10 min and is easily reproducible. These open-top devices are made of two layers: a first 1 mm-thick layer containing the structures and a 2 mm-thick reservoir layer to increase the volume capacity and prevent rapid evaporation of the culture media (*Movie SI.1*). The central chamber without the reservoir can only hold 7 µL, whereas it reaches a volume of 63 µL when the second layer is added. Due to the radial growth of axons in the DRGs, a circular central chamber with a diameter of 4 mm was designed to facilitate the penetration of axons into the microchannels **(Figure 1B)**. The central chamber is connected by 292 microchannels of 500 µm length, 10 µm width and 2.8 µm height to 6 peripheral chambers of 37 µL volume and 5 mm diameter. The dimensions of the microchannels have been chosen to enable compartmentalization of somas in the central chamber and axons in the peripheral chambers.[5,32] Treatments can be added in the outer chambers without flowing back to the central chamber. The high fluidic resistance of the microchannels creates a small but sustained flow between the chambers, thereby counteracting the diffusion (**Figure SI.3***)*. This fluidic isolation allowed 6 independent peripheral chambers to be created. The sTPE devices bond easily to polystyrene (PS) **(Figure 1C)**, making them adaptable to already existing basic culture plates. The Young's modulus of the SBC polymer is 1.15 MPa [27] which is in the same range as PDMS (0.5 – 3 MPa). In addition, this material is biocompatible, gas permeable, optically transparent and exhibits reversible bonding that can withstand 1 bar even after 10 sealing/unsealing cycles [30], making it a suitable candidate for cell culture. The air plasma hydrophilization remains stable in time for at least one week for the SBC chips. The culture of peripheral neurons was demonstrated using either explants or dissociated embryonic DRGs harvested from E13.5 mouse embryos. This model provides a solid experimental framework to study different aspects of Schwann cell development such as proliferation, migration, differentiation, and myelination of axons.[33] These co-cultures of neurons, Schwann cells and fibroblasts were placed directly into the central chambers and cultured within the SBC chips bonded to 6-well PS plates. The cultures were maintained for one month within the devices, and no leakage or contamination was observed. The reversible bonding properties of the SBC allowed the chips to be detached for cleaning and re-use.

2.2. A shear stress compatible with DRG culture

Fluid shear stress plays a key role in neural injury. It is essential to quantify the shear stress forces generated within the microchannels in order to evaluate the suitability of our device for biological studies. We used the Finite Elements Method (FEM) to visualize the speed v and the shear rate σ in a microchannel cross section **(Figure 2A)**, the two physical quantities being intrinsically linked by $\sigma = \mu \nabla v$. The following values were obtained for a pressure gradient of 30 Pa, which represents the theoretical maximum pressure that can be applied within the microfluidic device under study, given the finite volume of the reservoirs. The maximum shear stress inside the cross section is 0.8 dyn.cm^{-2}.

A pressure gradient of 30 Pa is achieved when the central chamber is full and the peripheral chambers are empty. However, this extreme case never occurs in practice when cells are in the chips. During the media change, the pressure reached a maximum of 25 Pa for a few seconds, due to the presence of a small volume of media within the chambers. Experimental validation was performed by measuring the time required for 0.2 µm microbeads to cross the microchannels **(Figure 2B)**. The experiment was started with a pressure of 25 Pa and stopped after 9 hours, when the pressure had reached 0 Pa. The flow rate (Q) inside the microchannels was calculated from the velocity of the microbeads and the area of the cross section of a microchannel (A): $Q = v \times A$. An exponential regression was fitted to the experimental results, with $v_{max} = 132{,}5 \mu m.s^{-1}$ and a time constant of $\tau = 3{,}18h$. It was then possible to derive the shear stress inside the microchannels based on the following equation: $\sigma = \frac{6\eta Q}{h^2 w}$, where η was fixed as the viscosity of water in Pa.s. For a maximum pressure of 25 Pa, the mean shear stress obtained was 2.73 dyn.cm^{-2}.

2.3. Viability and axonal growth

Embryos were harvested from pregnant mice at E13.5, a stage at which we can obtain a high yield of sensory neurons and Schwann cells, both of which exhibiting high viability and plasticity.[33] After the DRGs were picked from the extracted spinal cord, dissociated and seeded in PDMS and SBC chips, their viability was assessed at day *in vitro* (DIV) 3 and DIV7. For this, tiles of the central chamber were made using an epifluorescence microscope **(Figure 3A)** and all the cells were segmented and counted exhaustively (**Figure SI.6**). At DIV3, the cell density was below than the expected seeding cell density due to the low survival rate of the primary cells during the seeding step. The number of live cells was significantly higher in the control than in the chips **(Figure 3B)**. However, there was no significant difference in the number of dead cells between all the conditions. The proliferation rate was 13% in the control group between DIV3 and DIV7, compared to 64% in the PDMS chips. This rate was found to be similar between the SBC and the reused SBC chips, at 31% and 35% respectively. Similarly, DRG explants were fixed at DIV3, before the axons reached the microchannels, and at DIV7, after the axons had crossed the microchannels **(Figure 3C)**. The growth speed was deduced from the axonal length (**Figure SI.7**). Due to the fluidic isolation, the antibodies were unable to diffuse from the peripheral chambers into the microchannels. As the axons started to cross the microchannels around DIV4, it was necessary to detach the SBC chips at DIV7 before staining the cells to fully observe them in the peripheral chambers (**Movie SI.2***)*. However, it was not possible to properly detach the PDMS devices, so there was no result for axon length at DIV7 within them. No significant difference was observed between the axonal length in 4-well control and the axonal length in the chips **(Figure 3D)**. From DIV0 to DIV3, the axonal growth speed was 443±33 µm.day^{-1} and decreased to a speed of 324±36 µm.day^{-1} from DIV3 to DIV7.

2.4. SBC chips can be cleaned and re-used up to 3 times

A rapid, simple and reproducible protocol was developed to clean and reuse the chip **(Figure 4A)**. The process was completed in less than 3 min per device and required only milliQ water, soap, ethanol 70% and a toothbrush. Chips were sterilized again by UV-sterilization prior to culture. DRGs were grown up to one month in reused chips. It was confirmed that there was no noticeable difference in the surface of the SBC device before and after cleaning. Epifluorescence and SEM images were taken before use, after use and after the cleaning **(Figure 4B)**. Due to the sensitivity of the sTPE to electron beam, cracks appeared during SEM imaging. Using these two microscopy techniques, we confirmed that all the cellular debris present after culture had been removed by the cleaning protocol. After the third cleaning, it was observed that the axons were unable to enter the microchannels **(Figure 4C)**, suggesting that they were obstructed at the entrance. This finding was confirmed by optical profilometry measurement **(Figure 4D)**, which revealed that the microchannels were clogged. The clogging can be readily observed with a brightfield microscope (**Figure SI.9**) and is therefore easily detected. Consequently, each chip can be used up to 3 times before exhibiting irreversible deformation and becoming inoperable.

2.5. The reversible bonding of the SBC provides direct access to the cells

The reversible bonding properties and detachment of the SBC microfluidic chips also allowed direct access to the cells (*Movie SI.2*). Immunostaining of the cells was performed after the detachment of the device without damaging the cells **(Figure 5A)**. We can clearly observe axons and nuclei of Schwann cells and fibroblasts that had grown and migrated inside the microchannels. NFH is an anti-neurofilaments-heavy chain while SMI312 is staining the neurofilaments-medium chains (NFM) and NucRed the nuclei. Similar images were obtained on fixed cells by SEM after opening of the chips **(Figure 5B)**. The cells were not damaged by the detachment or the drying process required prior to metallization. The reversible bonding properties also allowed direct access to the cells, which could then be scraped in order to realize WB and RT-qPCR (see **Figure 5C-D**). WB was performed after 11 days of culture by scraping DRGs either from a 4-well plate or from a 6-well plate after detaching the SBC chips. Four DRGs were pooled together, and the results showed no significant difference in the expression of SOX10, a protein expressed in Schwann cells, between the DRGs extracted from the control and the SBC devices (**Figure 5C**). RT-qPCR was conducted on a single DRG explant scraped from a well or a chip after 7 days of culture. The expression of *krox20*, *mbp* and *dhh*, markers of the Schwann cell lineage, was found to be comparable in the control and in the SBC chips (**Figure 5D**).

2.6. Comparison of carbon footprint of SBC and PDMS chips fabrication process

The energy and time needed to assemble an SBC and a PDMS device were calculated at each stage of the fabrication process **(Figure 6A-B)**. The total energy required to fabricate an SBC chip was 289,3kJ,

almost 2 times less than the molding step of a PDMS chip alone, which required 556,8 kJ. PDMS chip fabrication took more time and consumed more supplies, resulting in more waste than an SBC chip. Moreover, an SBC device could be cleaned and reused 2 times before disposal. The cleaning step required no energy and took only 3 min, thereby reducing the time and energy needed for the fabrication process, as well as the cost and kg of CO2 generated **(Figure 6C** and **Table SI.1**). Compared to a PDMS chip, a reused SBC device took 4 times less energy and time to manufacture. The overall price for a single PDMS chip is €2.83, while the price of an SBC chip is €3.10. However, the price of the SBC device decreased to €1.72 when it was reused. To determine the carbon footprint generated by the SBC raw material production, we assumed that it was the average of the carbon footprint of polystyrene, polybutadiene and polyethylene production. The resulting value for one SBC chip is 0.013 kg CO_2e while for a PDMS chip it is 0.025 kg CO_2e. When an SBC device is reused, as there is no need for new SBC there is no more carbon footprint generated by the material fabrication. The overall carbon footprint has been calculated by considering the mass of CO_2 equivalent generated per chip for electricity consumption, polymer for chip and 6-well plate production, washing of the chip and disposal of the wastes by incineration. Most of the carbon footprint was attributed to the disposal and washing protocols and was similar for the three types of chips. However, the reused SBC devices produced 0.05 kg CO_2e less than the PDMS ones because they consumed less electricity and didn't require the production of polymer.

3. Discussion

The device has been designed with a central circular chamber to facilitate cell loading and the access to the microchannels. This geometry increases the accessibility of axons to the microchannel entrance as DRG explants have an anisotropic axonal growth. For dissociated DRGs, it has been described that the radial flow pressure resulting from the circular fluidic design facilitates the positioning of cells in close proximity to the microchannels inlet.[9,10,34] Moreover, the circular design allows for more than 3.5 times higher axon coverage compared to square designs.[9] Moreover, it allows the cultivation of both dissociated DRGs and explants while most of the DRGs cultured on chip are dissociated.

This design allows a homogeneous treatment in the central chamber, while a gradient treatment in the peripheral chambers, thanks to the high resistance of the microchannels. This feature can be useful for drug treatments, however it prevents antibodies to reach the microchannels during immunostaining constraining us to open the chip to observe the entirety of the axons. In addition, the open-top device facilitates media changes and the CO2 exchange, while reducing the mechanical stress and shear stress compared to a closed-compartment device.[19] The stable hydrophilization was especially convenient for transport and long-term use compared to PDMS. We compared the maximum shear stress value obtained in our device to the maximum shear stress value that is

sustainable for cortical neurons. We considered the value of 5 dyn.cm^{-2} which was measured for a 24h exposure[35] as a reference, as to our knowledge there are no data on the effect of shear stress on sensory neurons. The maximum experimental shear stress obtained in our device is 1.25 times higher than the maximum theoretical shear stress. However, it is almost 2 times lower than the cell viability limit for cortical neurons. It should be noted that the maximum shear stress in our device is only reached for a few seconds while the cells are inside, during the media change. We numerically confirmed that the axonal growth rate is not impacted by the microfluidic chip, assuming a comparable threshold in our biological context. To confirm the viability of the cells and ensure that our microfluidic architecture does not affect them, tiles of the central chambers of the chips and of the wells of the controls were made. The tiles allowed us to monitor viability over time and confirm the homogeneous spatial distribution of dead cells in the chips whereas in a standard well plate, cells tend to accumulate on the walls.

Even when using the same 3 mm puncher to open the central chamber of the SBC and PDMS chips, the diameters of the holes obtained are not the same (**Figure SI.2**). This is a consequence of the elongation at break of the SBC (720%) compared to the PDMS (76%) one.[26,30] As the diameters are different, the seeding area is different for both materials. We have a surface area of 7.1 mm^2 for SBC devices and 3.14 mm^2 for PDMS ones. We had to adjust the number of cells seeded for each material to keep the same seeding density. However, only the open top parts are different in size, the central chamber is still 4 mm in diameter for both materials, which explains why there are fewer cells per mm^2 in the PDMS devices than in the SBC devices. Moreover, after 3 days, the cell density was higher in the well plate than in the chips, suggesting that the dissociated cells tend to proliferate more when not confined by microchannels, where there is less renewal of medium. As there is a small flow between the chambers of the chips, the cells are in a less suitable environment than in a well plate. However, the proliferation rate in the chips is higher than in the control. As more cells survive the seeding process in the control, they reach confluence faster and therefore proliferate less.

The axonal growth rate in the chips is similar to the control, meaning that the presence of microchannels has no effect on axonal growth. It is also similar to that observed in the literature, with a rate of around 400µm/day.[36] The reused chips did not affect either cell viability or axonal growth rate, demonstrating that it is possible to reuse a chip in SBC for cell culture.

Many reversible bonding strategies have been recently reported, for applications going beyond cell culture.[29] Most of them require the intervention of an external help, a change in the design or the addition of an interlayer between the chip and the substrate. PDMS can be bonded reversibly without plasma treatment, but it is not easily reproducible and leakage occurs rapidly. Axons can grow under the microchannels rather than inside them and the hydrophobicity of the PDMS, which is usually made hydrophilic by plasma bonding, prevents liquid to easily entering the device.[28] The self-adhesive

properties of thermoplastic elastomers have also been used for reversible bonding [37] and their reported maximum working pressure without plasma bonding is 3.4 times higher than that of PDMS one.[38] The SBC we use has self-adhesive properties that do not require any external assistance or design changes. We have shown that it can be reused without impacting the cell culture and no leakage was observed. Axons grew inside the microchannels and the SBC chips were hydrophilized by using plasma treatment without impacting their reversible bonding. Cleaning the chips after use has been suggested before [39], but to our knowledge, has never been described. We proposed a fast and simple detailed protocol for cleaning the devices after use, thus enabling them to be reused. However, the reusability of the chips is limited in this particular context. After 3 uses, the microchannels were repeatedly clogged, completely blocking the flow between compartments. We hypothesize that this could be due to the uniform repetition of the different thermal cycles and plasma treatments, as the microchannels clogging was identical and regularly distributed. For chips with thicker channels (in this case the clogged channels were 2,8µm thick), it is possible to exceed the n = 3 limit.

Axons are not only growing inside the central chamber, but also in the reservoirs (**Figure SI.12**). When the chip is detached, these axons are teared at the same time. However, most of the axons present in the microchannels remain attached. They can be immunostained after fixation and the images were more contrasted and with a more uniform background than with the devices on due to the contribution of the autofluorescence of the polymer chip. This direct access allowed also to achieve direct collection for biological analysis of proteins (western blot), which has already been realized with device with a detachable substrate device [13], or nucleic acids (RT-qPCR), which has been carried out directly on the chip.[40] The detachment of the chips allowed easy scraping of the cells to collect most of the biological material. WB was performed on 4 DRGs pooled, experiments have been conducted on 1, 4 and 8 DRGs in controls to assess the number of DRGs necessary to extract sufficient proteins (**Figure SI.13**). The results showed that there was no significant difference by using 4 or 8 DRGs. However, there is almost 40% of signal intensity difference between the 1 DRG and 4 DRGs experiments, supporting our choice to pull 4 explants together. RT-qPCR was performed by pulling 1 or 2 DRGs explants and similar results were obtained, confirming that enough RNA was collected by scrapping 1 DRG to perform an experiment. Moreover, around 20 ng/µL of RNA was extracted from 1 DRG which would be sufficient to test approximatively 30 genes.

Time, energy and carbon footprint generated for SBC and re-used SBC chips fabrication were lower than for PDMS ones fabrication. PDMS required more material and thus generated more waste and cost. Thermoplastics were cheaper to produce[41] but because PDMS is produced in larger quantities, its final price is lower. It should be noted that the calculations are based on low carbon electricity, coming mostly from nuclear power plants. Depending on the country of reference, electricity can affect both the price and the carbon footprint. Costs and carbon footprint could be lowered for both SBC and

PDMS devices fabrication by reducing the amount of waste generated as they cause half of the mass of CO_2e produced. The quantities of ethanol and milliQ water could be minimized, and increasing the density of chips per mold would also reduce the amount of energy and time necessary to produce them. However, the amount of wasted SBC is easier to reduce than for PDMS because the SBC can be cut to the desired size whereas PDMS must be poured over the entire surface of the mold. When comparing all the environmental impacts from cradle to grave, normalized to those of PDMS, SBC and reused SBC chips appeared to be lower for all impacts, in particular for marine eutrophication and mineral resource scarcity (*Table SI.2*), confirming the interest of using SBC as an alternative to PDMS. In our work, we choose to focus only on the manufacturing process for comparison purposes. However, the total energy required to produce one chip can be considered negligible when compared to the energy consumed in the lab or the energy required to produce and transport the material [42–44]. If we considered the fabrication of 300 chips over a year, the carbon footprint associated with chip fabrication corresponded to 1/60th of the mean carbon footprint of one researcher in one year (6teq CO_2[42]). In summary, the SBC already shows a very interesting reduction in time and cost for the prototyping phase and could have a significant impact on the environmental impact of a product on an industrial scale. This analysis underlines the importance of quantifying and optimizing the environmental impact of microfluidic devices, especially in a field where there is an ongoing industrial scale-up that should intensify with the growing rationalization of animal models.

Our device provides the possibility to study the neuronal functions and structures, featuring a pioneering material and architectural design in microfluidics systems for neuroscience applications. It is taking part in the recent evolution of microfluidic devices to accelerate the clinical translation of therapeutics for neuropathologies.[45,46]

4. Conclusion

We introduced a detachable, reusable, easy to produce and equivalent in cell culture performance SBC device for an original application to DRGs culture in the context of peripheral nervous system study. We proposed a new design adapted to DRGs explants and their radial growth with 6 peripheral compartments. We estimated the shear stress in the chip and experimentally confirmed its ability to perform axonal growth and viability assays of a murine peripheral nervous system model. Control with PDMS devices, which are the most commonly used devices to grow neurons in a chip, and well plate culture showed equivalent performance based on the above biological assays. The demonstration of growth and maintenance of a primary co-culture of nerves, which are particularly sensitive to stress, in an SBC chip paves the way for tissue diversification and species growth in SBCs for the neurofluidic community, but more generally for the microphysiological systems community. The reversible bonding

of the chips has been exploited both for direct access to different contact imaging microscopy and biological analysis techniques such as SEM, WB and RT-qPCR. The possibility to recycle our chips led us to develop an original workflow to evaluate the resources (time, energy, financial costs and CO2) involved in the production and recycling of the chip, which could be used by the microfluidic community in general to initiate a deeper rethinking. Switching to a reusable SBC chip allowed a significant reduction in all these resources, more than 4 times in time and energy compared to PDMS, contributing to more sustainable research. In the field of MPS, this paradigm shift illustrated by our device and workflow makes it possible to derisk device development for academic laboratories with limited resources, as well as reducing the impact of a rapidly growing industry.

From an animal ethics perspective, the development of alternative *in vitro* models has the potential to significantly reduce the animal use, in alignment with the 4Rs commitment. In the case of DRGs, the number of embryos in a pregnant mouse is typically between five and seven, with an average of 40 DRGs per embryo. This yields a potential 250 experiments to be conducted from a single mouse, depositing one dorsal root ganglion per chip. This approach allows for the testing of up to 1,500 conditions using the proposed design, rendering it highly valuable for drug screening and mechanistic investigation studies.

5. Experimental Section

5.1. Chip design and fabrication

5.1.1 Molds fabrication

The photomask designs were drawn using CleWin 5.2.4 version and printed on a SodaLime substrate with a resolution of 128k dpi (JD Photo Data, UK). A first layer of 2.8 µm thick microchannels was structured with SU-8 2002 (Chimietech, France) on a 4-inch diameter silicon wafer 1mm thick using soft lithography. This was followed by the addition of a second layer of 100 µm thick chambers made with SU-8 2050 (Chimietech, France). The Epoxym Kit (EdenTech, France) was used to create a negative replica in 1:10 Sylgard 184 PDMS (Neyco, France), followed by an epoxy positive replica of the SU-8 mold with Gallon KIT Conapoxy FR-1080 (Ellsworth Adhesives, USA).

a) Thermomolding and assembly of SBC chips

The microfluidic chips were embossed from styrene block copolymer (SBC) foils (EdenTech, France) at 160°C for 3 min (0.07-0.08 MPa) using the Sublym hot press machine (EdenTech, France) and the previously fabricated epoxy mold. The central chamber was punched with a 3 mm punch to obtain an open top device. A second layer of SBC embossed on a flat epoxy mold was added to each chip with a 6 mm diameter reservoir for the central chamber. The outer chambers were punched simultaneously

in the patterned layer and the reservoir layer using a 4 mm puncher. Finally, each chip was die-cut with a 26 mm puncher. The two-layer devices were then placed in a 6-well plate (VWR, USA) for hydrophilization by plasma treatment for 10 minutes in a plasma cleaner/sterilizer (Harrick Scientific Products, USA). They were baked at 80°C for 2 hours to increase the bonding strength.

b) Fabrication and assembly of PDMS chips

Polydimethylsiloxane (PDMS) chips and reservoirs were respectively molded with 1:10 Sylgard 184 from the SU-8 mold and a basic silicon wafer, and baked at 80°C for 2 hours. The patterned layer and the reservoir layer were punched with the same punchers used for the SBC chips and both were plasma treated for 10 min prior to assembly. 6-well plates were pre-treated with 1% (3-aminopropyl)triethoxysilane (APTES, Sigma-Aldrich, Germany) in milliQ water. Finally, the devices were treated with plasma again for 10 minutes and were bonded in the 6-well plates.

c) Sterilization and coating of the chip

The same protocol was used on the SBC and PDMS chips. The plates containing the devices were placed in a UV/Ozone ProCleaner™ Plus (BioForce Nanosciences, USA) for 10 min for sterilization. The chips were then rinsed with EtOH 70% and three times with Dulbecco's phosphate buffered saline 1X (D-PBS 1X, Gibco, USA) before being incubated with 5% Poly-L-lysine (Sigma-Aldrich, Germany) in a solution of boric acid (Sigma-Aldrich, Germany) and sodium hydroxide for 30 min at 37°C. After washes with Neurobasal medium (Gibco, USA), they were coated with a solution of 130 $\mu g.ml^{-1}$ rat tail collagen I (Clinisciences, France) in 17.5mM acetic acid for 1h at room temperature. Finally, the chips were rinsed again and placed at 37°C and 10% CO_2 overnight before cell seeding. The same coating procedure was followed for the 4-well and 96-well plates, which were used as controls.

d) Detachment and cleaning of the chip

The wells were filled with 1 mL of D-PBS to immerge the chips before to progressively detach them with a tweezer. After 10 min of incubation at room temperature, the chips were carefully removed from the wells. If cells observation was not needed, the devices were detached directly without the incubation step. To clean them, they were first bathed in a solution of milliQ water and soap solution and gently brushed with a toothbrush, then rinsed successively with milliQ water, EtOH 70% and with milliQ water again. Finally, they were either dried in a laminar flow hood for 1h before storage or dried with compressed air and directly reused following the usual protocol of sterilization and coating. Optical profilometry was performed with a WykoNT9100 optical profilometer (Veeco, USA) on a new chip and a chip that had been used up to 4 times and cleaned each time.

5.2 Dorsal Root Ganglia (DRG) Cell Culture

a) Cells harvesting, seeding and maintenance

Dorsal root ganglia (DRGs) were harvested from embryos at E13.5 surgically removed from pregnant C57BL/6 J mice (Janvier, France) following a previously described protocol.[47] For explant culture, the devices were filled with DRG plating media (DMEM high glucose (Gibco, USA), Glutamax 1X (Gibco, USA), 10% Heat Inactivated Horse Serum (Gibco, USA), 2.5S NGF (R&D Systems, USA), Antibiotic/Antimycotic 1X (Gibco, USA)). One DRG was placed in the central chamber of each microfluidic chip or in the center of a well of a 4-well plate. For dissociated cell culture, the DRGs were trypsinized with a solution of 0.25 Trypsin in Hanks' Balanced Salt Solution 1X (HBSS 1X, Gibco, USA) for 30 min at 37°C and 5% CO_2. Trypsinization was stopped with L-15 media (Gibco, USA) containing 10% horse serum. DRGs were then spun down at 1,500 rpm for 5 minutes. The cells were resuspended in DRG plating medium and seeded at a targeted density of 275 000 cells.cm^{-2} inside the central chambers or in a 96-well plate. The dissociated cells were seeded in a volume of 7µL in the central chamber and incubated 2 hours prior to fill the reservoir, to allow them to adhere to the surface of the culture plate. DRGs were incubated at 37°C and 10% CO_2. 18 to 20 hours after the seeding, the medium was replaced with Neurobasal medium supplemented with Glutamax 1X, 2.5S NGF, B27 Supplement (Gibco, USA) and Antibiotic/Antimycotic 1X. The medium was changed every 2 days. To prevent evaporation, 3 mL of D-PBS was added in between the wells of the plates. All aspects of animal care and animal experimentation were performed in accordance with the relevant guidelines and regulations of INSERM and Université Paris Cité (authorization APAFIS#7405-2016092216181520).

b) Live and dead cell assays

Viability was assessed at day *in vitro* (DIV) 3 and DIV7 using a LIVE/DEAD Viability/Cytotoxicity Assay Kit (Invitrogen, USA). Cells were incubated for 30 min at 37°C and 10% CO_2 and rinsed with L15 medium without red phenol (Gibco, USA). Cells were observed using the Cy5 and EGFP channels on a ZEISS Axio Observer Z1 microscope (Zeiss, Germany) incubated at 37°C and 10% CO_2 and the images were processed using ImageJ 1.54j.[48] The data obtained were analyzed using R and tidyverse and the graphs were plotted on GraphPad Prism 8 (GraphPad Software, USA). The full R markdown script is available as supplementary information (*Script SI.1*). Sidak's multiple comparison tests were performed. The alpha value threshold was set at 5% and the *P*-values are presented as follows: $*P < 0.05$, $**P < 0.01$, $***P < 0.001$.

c) Immunostaining

Cell cultures at DIV3 and DIV7 were fixed with 4% paraformaldehyde (PFA, Electron Microscopy Sciences, USA) for 10 min at room temperature. At DIV7, the SBC chips were detached to facilitate the staining. The cells were then permeabilized (0.25% Triton X100 (Sigma-Aldrich, Germany) and 0.1% Tween20 (Thermo Fischer Scientific, USA) in D-PBS) for 10 min. After washes with D-PBS and incubation

for 45 min in a blocking solution (0.5% Triton X100, 0.1% Tween20, 2% bovine serum albumin (BSA, Sigma-Aldrich, Germany), 3% Mouse on Mouse blocking reagent (Bio-Techne, USA) and 5% Normal Donkey Serum (Sigma-Aldrich, Germany)), the cells were incubated overnight at 4°C with the primary antibodies: rabbit anti-NFH (1:1000, Merck Millipore Ref. AB1989, Germany) and mouse anti-SMI312 (1:250, BioLegend Ref. AB_2566782, USA). The cultures were again rinsed with D-PBS and incubated for 1h at room temperature with the secondary antibodies: donkey anti-rabbit Alexa Fluor™ 488 (1:1000, Invitrogen Ref. A-21206, USA) and donkey anti-mouse Cyanine3 (1:165, Jackson Ref. AB_2340813, USA). For nuclear staining, the devices were incubated 30 min in a solution of NucRed (Invitrogen, USA) in HBSS. To reduce the amount of antibody and staining required for chip detachment, rings were 3D printed in polylactic acid and placed in each well to reduce the surface area (**Figure SI.1-2**). Images were captured on a ZEISS Axio Observer Z1 microscope and processed on ImageJ using the *NeuriteJ* plug-in. The resulting data were processed in RStudio (Posit, USA) and graphs plotted on GraphPad Prism 8. The full R markdown script is available as supplementary information (**Script SI.2**) Sidak's multiple comparison tests were performed.

d) Western Blot

Western blots (WB) were performed on DRGs explant cultures at DIV11. The chips were detached, and the proteins were extracted by scraping the DRGs in RIPA buffer (50mM Tris Base, 150 mM NaCl, 1mM $MgCl_2$, 1% NP-40 (Sigma-Aldrich, Germany), 0.1% sodium dodecyl sulfate SDS (EU0660, Euromedex, France), 0.5% sodium deoxycholate (D6750, Sigma-Aldrich, Germany), Protease Inhibitor Complete mini EDTA free (11836170001, Roche, Switzerland), Pyrophosphate (10mM, S9515, Sigma-Aldrich, Germany), Phosphate Inhibitor Cocktail 2 (10µL/ml, P5726, Sigma-Aldrich, Germany), Phosphate Inhibitor Cocktail 3 (10µL/ml, P0044, Sigma-Aldrich, Germany) and sodium fluoride (10 mM, S7920, Sigma-Aldrich, Germany)). The protein quantification was determined using a Bio-Rad DC Protein Assay (Bio-Rad, USA) with BSA as the standard. A total of 15 µg of protein was loaded into a 4-20% TGX 10-wells gel (Bio-Rad, USA) and the transfer step was performed using a Trans-Blot Turbo transfer system (Bio-Rad, USA) on polyvinylidene difluoride membranes (Bio-Rad, USA). Non-specific binding sites were blocked with blocking solution (5% BSA in Tris Buffered Saline (TBS, Euromedex, France) and then incubated with primary antibodies rabbit anti-Sox10 (1:1000, ab155279, Abcam, UK) and rabbit anti-Actin (1:2 000, ab8227, Abcam, UK), followed by a goat anti-rabbit Horseradish Peroxidase (HRP) coupled secondary antibody (1:20 000, 111-035-144, Jackson IR, UK). Finally, specific bands were detected with the Pierce®ECL 2 Western Blotting substrate kit (RPN2209, Thermo Fischer Scientific, USA), using the ImageQuant LAS 4000 ECL imaging system (GE Healthcare, USA). The images were analyzed using the gel tool analyzer of ImageJ (1.54g). The integrated densities of Sox10 were

normalized to β-actin expression and plotted using GraphPad Prism 10. A t-test was performed for statistical analysis.

e) RT-qPCR

RT-qPCR was performed on explants at DIV7. The chips were detached and the DRGs were scraped in Trizol (15596018, Invitrogen, USA). The RNA was precipitated and resuspended in water prior to quantification with a Nanodrop (Thermo Fischer Scientific, USA). The SuperScript III Reverse Transcriptase (18080085, Invitrogen, USA) was used following the manufacturer's instructions to realize the reverse transcriptase of 90 ng of RNA. qPCR was performed on a CFX384 biorad qPCR machine (15s of denaturation at 95°C, 30s of elongation at 60°C – 40 times) by using Sybr Green Rox kit (AB-1162/B, Thermo Fischer Scientific, USA) containing 300 nM of selected primers (**Table 1**). The quality of the qPCR was tested by checking the dissociation curve. Each qPCR reaction was performed in triplicates. Relative expression of target genes were normalized to Ppia and Rpl13a mRNA levels and calculated using the ΔΔCt. Results are expressed as fold changes with respect to the controls and the data were plotted using GraphPad Prism 10.

Gene	Sequence 3'-> 5'	Sequence 5'->3'
Ppia	GGCAAATGCTGGACCAAAC	CATTCCTGGACCCAAAACG
Rpl13a	TACGCTGTGAAGGCATCAAC	TTGGTATTCATCCGCTTCCG
Krox20	TGCACCTAGAAACCAGACCTTC	TGCCCGCACTCACAATATTG
Mbp	ACTCACACACGAGAACTACCC	GGTGTTCGAGGTGTCACAATG
Dhh	ATCCACGTATCGGTCAAAGC	AGTCACCACGATGTAGTTCCC
B-actin	ATGGTGGGAATGGGTCAGAAG	TGCCATGTTCAATGGGGTAC
Pgk1	ACGGTGTTGCCAAAATGTCG	TTGGAACAGCAGCCTTGATC
Gapdh	GTGGACCTCATGGCCTACAT	TGTGAGGGAGATGCTCAGTG

Table 1: qPCR primers used in this study

f) Scanning Electron Microscopy

After 21 days of culture, the cells were rinsed with D-PBS and fixed in 4% PFA. The bottom of each well was then laser-cut using a Universal Laser Systems VLS 4.60 (Universal Laser Systems, Inc., USA) to obtain circular slides suitable for scanning electron microscope. The chips were detached according to the previous protocol and the biological samples were dried using an automated critical point dryer Leica EM CPD300 (Leica Microsystems, France). The samples were then metallized with platinum in a

Cressington 208HR metallizer (Cressington Scientific Instruments, UK) and observed in a Zeiss Gemini SEM 360 scanning electron microscope (Zeiss, Germany).

g) Finite Element Method (FEM)

COMSOL Multiphysics software was used to perform diffusion-convection simulations on the microfluidic device. The *creeping flow* and *transport of diluted species* modules were implemented for this study. In the diffusion-convection experiment, a pressure gradient of 5 and 20 Pa between the inlet and the outlet was used for the convective flow, and an inflow of 0.5 mM of water (diffusion coefficient D = 10^{-9} $m^2.s^{-1}$) was used for diffusion, by keeping the inlet and outlet the same (transport) or opposite (isolation). The system comprises two identical blocks of size 1 x 1 x 0.1 mm^3, merged with a smaller block of size 0.5 x 1 x 0.028 mm^3. This geometry represents the junction between the central and peripheral chambers, which is of particular relevance for the study. Approximate solutions of the following equations were numerically calculated by the FEM software:

$$\rho \frac{\partial u}{\partial t} = \nabla \cdot [-pI + \mu(\nabla u + (\nabla u)^T)] + F \quad (1)$$

$$\rho \nabla \cdot u = 0 \quad (2)$$

$$\frac{\partial c_i}{\partial t} + \nabla \cdot J_i + u \cdot \nabla c_i = R_i \quad (3)$$

$$J_i = -D_i \nabla c_i \quad (4)$$

Equation (1) is the Navier-Stokes equation, (2) is the incompressibility of the flow, (3) is the diffusion-convection equation, and equation (4) is Fick's law of diffusion with ρ the fluid density, u the fluid velocity, p the fluid pressure, I the identity matrix, T the temperature, μ the fluid dynamic viscosity, F the external forces applied to the fluid, and where, for species i, c_i is the concentration, J_i is the molar flux, R_i is a net volumetric source for *c* and D_i is the diffusion coefficient.

h) Particle image velocimetry

The devices were first coated with 5% BSA in D-PBS1X for 10 min to reduce collision impact with the walls. FluoSpheres™ amine (0.2 µm diameter) (Invitrogen, USA) were diluted 1/40000 in the same solution. To obtain a flow of 25 Pa, 60 µL of the microbead solution was injected into the central chamber and 5 µL of the solvent solution was injected into the peripheral chambers. D-PBS was added in between the wells to prevent evaporation and the plate was sealed with parafilm. Microbeads were observed using the Cy5 channel on a ZEISS Axio Observer Z1 microscope. Images were analyzed directly using the Zeiss Zen software and data were plotted using GraphPad Prism 8.

i) Time, cost, carbon footprint and energy consumption calculations

The estimated times, costs, carbon footprint and energy consumption were calculated for one chip. Power consumption was measured using a wattmeter Primera-Line PM 231 E (Lextronic, France). The measurements were converted to energy by multiplying the power by the time of use of each piece of equipment. Whenever an equipment was used for several devices at the same time, the amount of energy and time were divided by the number of chips to estimate the amount required for one device. Material prices were based on supplier prices. Electricity prices were based on the French electricity price in June 2024 (€0.2516/kWh). The carbon footprint was calculated based on the direct emissions of products manufactured in Europe, using the Ecoinvent 3.5 database, required for the fabrication of one chip. PDMS production was assimilated to silicone using the Ecoinvent process 'product production | silicone product | APOS, S RER', while SBC manufacture was modeled as an average of 25% polyethylene, 25% polybutadiene and 50% polystyrene using the processes 'polyethylene production, high density, granulate | polyethylene, high density, granulate | APOS, S, RER', 'polybutadiene production | polybutadiene | APOS, S, RER' and 'polystyrene production, general purpose | polystyrene, general purpose | APOS, S, RER'. In addition, the impact calculations included electricity consumption, 6-well plate production, washing protocol and waste disposal by incineration. Impacts were calculated using the ReCiPe 2016 Midpoint (H) method.

Data availability

The data for this article plots can be found on https://github.com/HugoSalmon/25Moreau .

Supporting Information

Supporting Information is available from the Wiley Online Library.

Acknowledgements

S.B. and H.S. contributed equally to this work. This research was funded by the French National Research Agency (ANR-23-CE19-0007-01) and the Université Paris Cité via the Initiative d'Excellence Idex Emergence (IDXD7-MOCHI). The motorized microscope and the motorized macroscope were funded by DIM BIOCONVS Région Ile de France (HCS-Mochi and MisoSoup projects, respectively). RFB was funded by DIM ELICIT Région Ile de France (FOMO project). We thank L. Réa from UMR 7057 MSC for prototyping the microscope adaptor.

S.M., S.B. and H.S. acknowledge T. Bastien at the mechanical workshop core facility of BioMedTech Facilities Université Paris Cité for the 3D prototyping. The authors thank the staff of UMR 7162 MPQ clean room, the IPGG platform for the easy access to the platform and ITODYS platform from Université Paris Cité) for the SEM images. Finally, the authors thank V. Sundaram and C. Massaad for the discussions regarding the peripheral nerve modeling, J-M Di Meglio and Dmitri Ayollo for discussions on microscopy.

Conflict of Interest

The authors declare no conflict of interest.

Received:

Revised:

Published online:

List of abbreviations

4R: Reduction, Replacement, Refinement and Responsibility

CNS: Central Nervous System

DIV: Days *in vitro*

DRG: Dorsal Root Ganglia

PDMS: PolyDiMethylSiloxane

PNS: Peripheral Nervous System

RT-qPCR: Reverse Transcription quantitative Polymerase Chain Reaction

SBC: Styrenic Block Copolymer

SEM: Scanning Electron Microscope

sTPE: soft Thermoplastic Elastomer

WB: Western Blot

References

1 A. D. Jadhav, L. Wei and P. Shi, *Curr. Neuropharmacol.*, 2016, **14**, 72–86.
2 F. M. Pramotton, S. Spitz and R. D. Kamm, *Adv. Sci.*, 2024, **11**, 2403892.
3 T. Osaki, Y. Shin, V. Sivathanu, M. Campisi and R. D. Kamm, *Adv. Healthc. Mater.*, 2018, **7**, 1700489.
4 R. B. Campenot, *Proc. Natl. Acad. Sci.*, 1977, **74**, 4516–4519.
5 A. M. Taylor, M. Blurton-Jones, S. W. Rhee, D. H. Cribbs, C. W. Cotman and N. L. Jeon, *Nat. Methods*, 2005, **2**, 599–605.
6 A. J. Samson, G. Robertson, M. Zagnoni and C. N. Connolly, *Sci. Rep.*, 2016, **6**, 33746.
7 J. Courte, R. Renault, A. Jan, J.-L. Viovy, J.-M. Peyrin and C. Villard, in *Methods in Cell Biology*, eds. D. A. Fletcher, J. Doh and M. Piel, Academic Press, 2018, vol. 148, pp. 71–95.
8 A. D. Sharma, L. McCoy, Elizabeth Jacobs, E. R. Jacobs, H. E. Willey, J. Q. Behn, H. P. T. Nguyen, Brad Bolon, B. Bolon, J. L. Curley and M. J. Moore, *Sci. Rep.*, 2019, **9**, 8921–8921.
9 J. Park, H. Koito, J. Li and A. Han, *Biomed. Microdevices*, 2009, **11**, 1145–1153.
10 J. Park, H. Koito, J. Li and A. Han, *Lab. Chip*, 2012, **12**, 3296–3304.
11 B. Luo, A. P. Tiwari, N. Chen, S. Ramakrishna and I. H. Yang, *ACS Appl. Bio Mater.*, 2021, **4**, 8424–8432.
12 M. Shi, D. Majumdar, Y. Gao, B. M. Brewer, C. R. Goodwin, J. A. McLean, D. Li and D. J. Webb, *Lab. Chip*, 2013, **13**, 3008–3021.
13 S. Hyung, S.-R. Lee, J. Kim, Y. Kim, S. Kim, H. N. Kim and N. L. Jeon, *Sci. Adv.*, 2021, **7**, eabd9749.
14 S. Hyung, B. Yoon Lee, J.-C. Park, J. Kim, E.-M. Hur and J.-K. Francis Suh, *Sci. Rep.*, 2015, **5**, 15122.
15 R. M. Huval, O. H. Miller, J. L. Curley, Yuwei Fan, Y. Fan, B. J. Hall and M. J. Moore, *Lab. Chip*, 2015, **15**, 2221–2232.
16 I. H. Yang, Devin S. Gary, D. S. Gary, M. Malone, M. Malone, S. Dria, T. Houdayer, Thierry Houdayer, Visar Belegu, V. Belegu, J. W. McDonald and N. V. Thakor, *Neuromolecular Med.*, 2012, **14**, 112–118.
17 M. Malone, D. Gary, I. H. Yang, A. Miglioretti, T. Houdayer, N. Thakor and J. McDonald, *Glia*, 2013, **61**, 843–854.
18 H. U. Lee, A. Blasiak, D. R. Agrawal, D. T. B. Loong, N. V. Thakor, A. H. All, J. S. Ho and I. H. Yang, *PLOS ONE*, 2017, **12**, e0179642.
19 M. Ristola, L. Sukki, M. M. Azevedo, A. I. Seixas, J. B. Relvas, S. Narkilahti and P. Kallio, *J. Micromechanics Microengineering*, 2019, **29**, 065009.
20 N. Vysokov, S. B. McMahon and R. Raouf, *Sci. Rep.*, 2019, **9**, 12915.
21 S. M. Caparaso, A. L. Redwine and R. A. Wachs, *J. Biomed. Mater. Res. B Appl. Biomater.*, 2023, **111**, 1903–1920.
22 L. Kramer, *ALTEX*, DOI:10.14573/altex.2001181.
23 P. Khoshakhlagh, A. Sivakumar, L. A. Pace, D. W. Sazer and M. J. Moore, *J. Neural Eng.*, 2018, **15**, 064001.
24 C. Mutschler, S. V. Fazal, N. Schumacher, A. Loreto, M. P. Coleman and P. Arthur-Farraj, 2023, preprint, DOI: 10.1101/2023.05.19.541371.
25 J. W. Park, H. J. Kim, J. H. Byun, H. R. Ryu and N. L. Jeon, *Biotechnol. J.*, 2009, **4**, 1573–1577.
26 E. Berthier, E. W. K. Young and D. Beebe, *Lab. Chip*, 2012, **12**, 1224–1237.
27 J. Lachaux, C. Alcaine, B. Gomez-Escoda, C. M. Perrault, D. O. Duplan, P.-Y. J. Wu, I. Ochoa, L. Fernández, O. Mercier, D. Coudreuse and E. Roy, *Lab. Chip*, 2017, **17**, 2581.
28 J. Harris, H. Lee, B. Vahidi, C. Tu, D. Cribbs, C. Cotman and N. L. Jeon, *JoVE J. Vis. Exp.*, 2007, e410.
29 Y. Zhang, K. Sun, Y. Xie, K. Liang, J. Zhang and Y. Fan, *Rev. Sci. Instrum.*, 2023, **94**, 061501.
30 H. Salmon, M. R. Rasouli, N. Distasio and M. Tabrizian, *Eng. Rep.*, **n/a**, e12361.
31 M. D. Paepe, L. Jeanneau, J. Mariette, O. Aumont and A. Estevez-Torres, *PLOS Sustain. Transform.*, 2024, **3**, e0000116.
32 B. G. C. Maisonneuve, A. Batut, C. Varela, J. Vieira, M. Gleyzes, J. Rontard, F. Larramendy and T. Honegger, *Neurite growth kinetics regulation through hydrostatic pressure in a novel triangle-shaped neurofluidic system*, Neuroscience, 2021.

33 V. K. Sundaram, T. El Jalkh, R. Barakat, C. J. I. Fernandez, C. Massaad and J. Grenier, *Front. Cell. Neurosci.*, 2021, **15**, 590537.
34 S. Hosmane, I. H. Yang, A. Ruffin, N. Thakor and A. Venkatesan, *Lab. Chip*, 2010, **10**, 741–747.
35 M. Liu, W. Song, P. Li, Y. Huang, X. Gong, G. Zhou, X. Jia, L. Zheng and Y. Fan, *PLOS ONE*, 2013, **8**, e63473.
36 A. M. Conti, S. Brimijoin, L. J. Miller and A. J. Windebank, *Neurobiol. Dis.*, 2004, **15**, 106–114.
37 D. Brassard, L. Clime, K. Li, M. Geissler, C. Miville-Godin, E. Roy and T. Veres, *Lab. Chip*, 2011, **11**, 4099–4107.
38 B.-U. Moon, K. Morton, K. Li, C. Miville-Godin and T. Veres, *Processes*, 2021, **9**, 54.
39 M. Samandari, L. Rafiee, F. Alipanah, A. Sanati-Nezhad and S. H. Javanmard, *Sci. Rep.*, 2021, **11**, 10310.
40 X. M. Spijkers, S. Pasteuning-Vuhman, J. C. Dorleijn, P. Vulto, N. R. Wevers and R. J. Pasterkamp, *Sci. Rep.*, 2021, **11**, 2080.
41 E. Roy, M. Geissler, J.-C. Galas and T. Veres, *Microfluid. Nanofluidics*, 2011, **11**, 235–244.
42 A. Estevez-Torres, F. Gauffre, G. Gouget, C. Grazon and P. Loubet, *ChemRxiv*, 2023, preprint, DOI: 10.26434/chemrxiv-2023-6tt1w.
43 A.-L. Ligozat, C. Brun, B. Demirdjian, G. Gouget, E. Jardé, A. Mialon, A.-S. Mouronval, L. Pagani and L. Vieu, *bioRxiv*, 2024, preprint, DOI: 10.1101/2024.03.11.584380.
44 O. Ragueneau and A. Sabbagh, *One Earth*, 2024, **7**, 747–750.
45 J. Kajtez, S. Buchmann, S. Vasudevan, M. Birtele, S. Rocchetti, C. J. Pless, A. Heiskanen, R. A. Barker, A. Martínez-Serrano, M. Parmar, J. U. Lind and J. Emnéus, *Adv. Sci.*, 2020, **7**, 2001150.
46 S. Bang, S. Na, J. M. Jang, J. Kim and N. L. Jeon, *Adv. Healthc. Mater.*, 2016, **5**, 159–166.
47 C. Taveggia and A. Bolino, in *Myelin: Methods and Protocols*, ed. A. Woodhoo, Springer, New York, NY, 2018, pp. 115–129.
48 J. Schindelin, I. Arganda-Carreras, E. Frise, V. Kaynig, M. Longair, T. Pietzsch, S. Preibisch, C. Rueden, S. Saalfeld, B. Schmid, J.-Y. Tinevez, D. J. White, V. Hartenstein, K. Eliceiri, P. Tomancak and A. Cardona, *Nat. Methods*, 2012, **9**, 676–682.

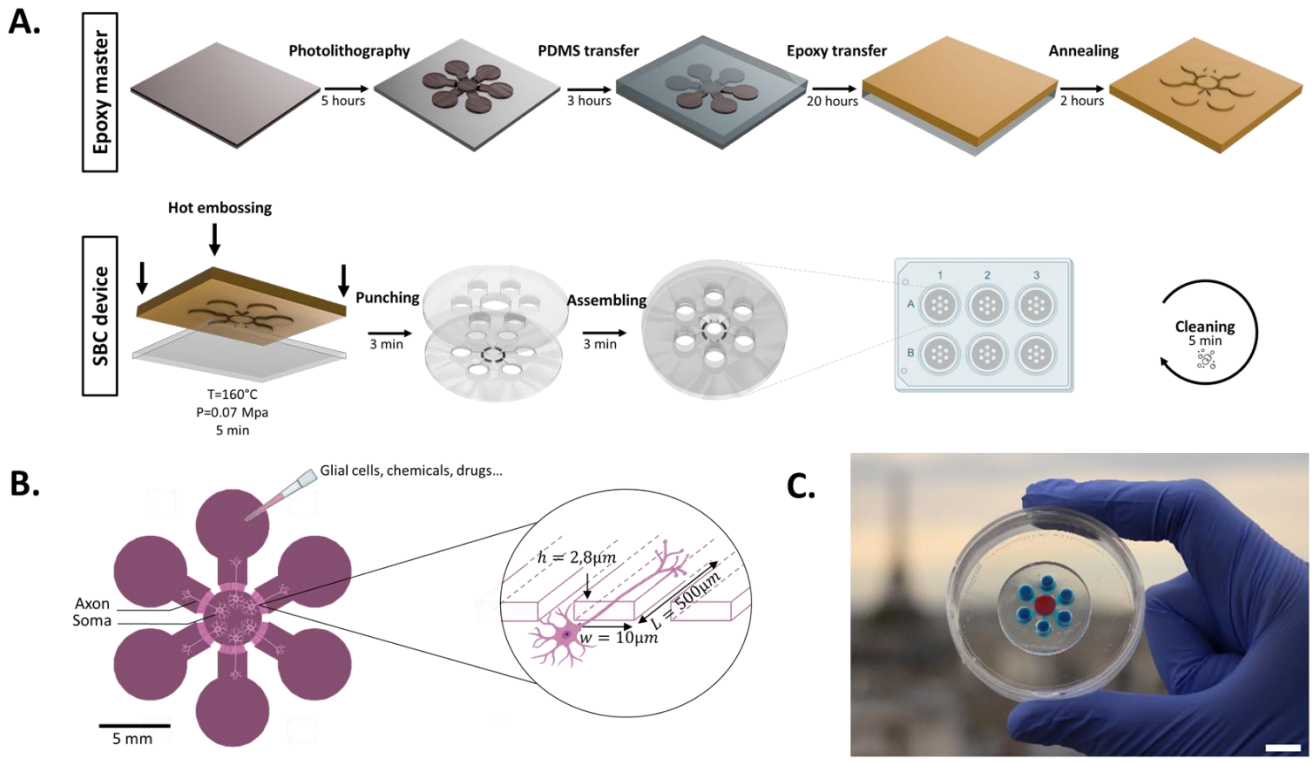

Figure 1: Fabrication and design of the thermoplastic chip. A. Fabrication process of the two-layer microfluidic chip in styrenic bloc copolymers (SBC). **B.** Scheme of the design of the chip. Somas are compartmentalized in the central chamber, while axons grow through the 292 microchannels. **C.** Image of the device filled with food dyes. Scale bar = 1cm.

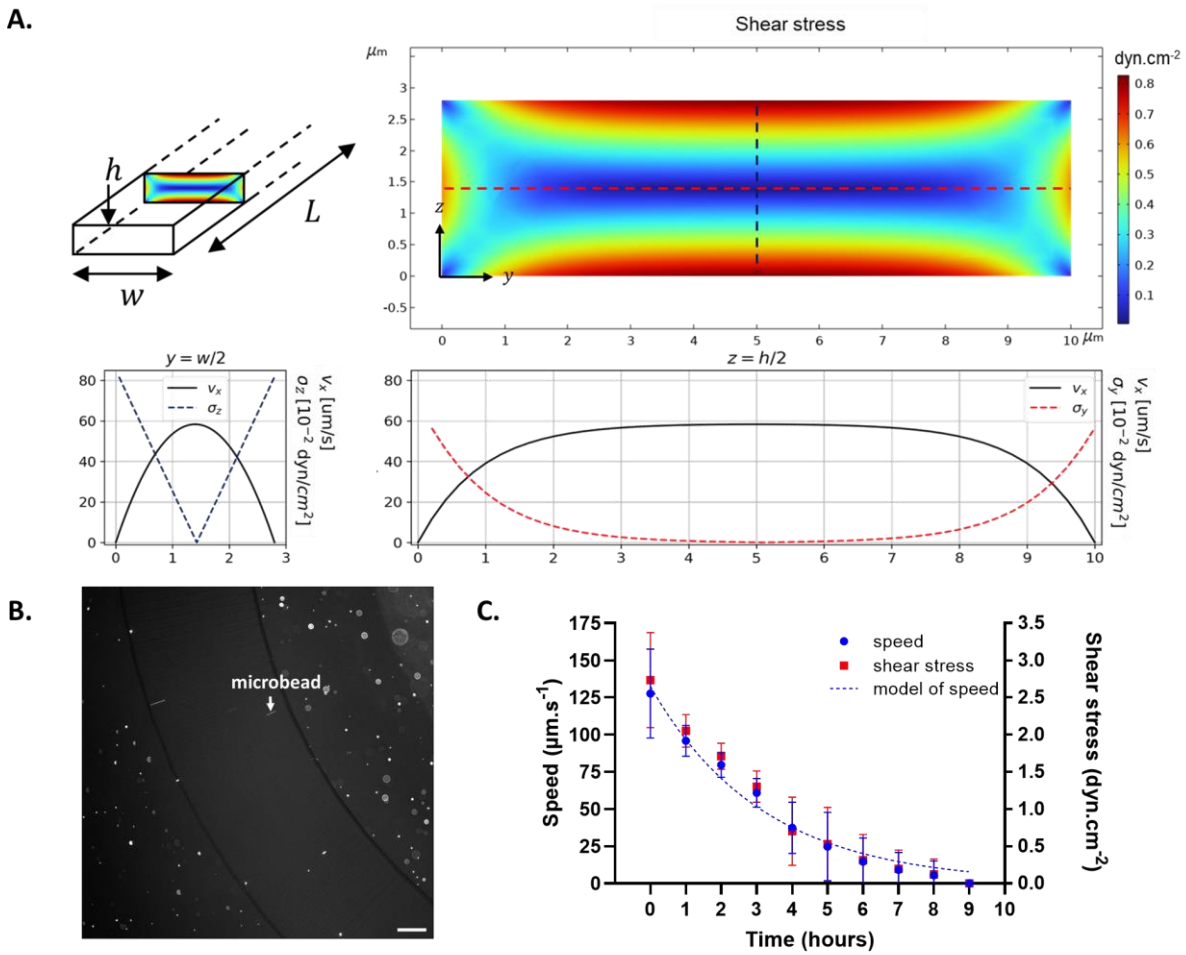

Figure 2: Estimation of the shear stress inside microchannels. A. Shear stress field induced by a 30Pa flow over a microchannel cross-section calculated by FEM, with associated analytical plots of the velocity (in black) and shear stress along the y-axis (dashed red line) and along the z-axis (dashed blue line). **B.** Particle image velocimetry in the chip of 200 nm fluorescent polystyrene particles. Scale bar = $100\ \mu m$ **C.** Evolution of the flow average speed inside the microchannels (blue curve), fitted exponential model for the average flow speed (dotted blue line), and associated shear stress (red curve) over time for initial pressure conditions of 25 Pa.

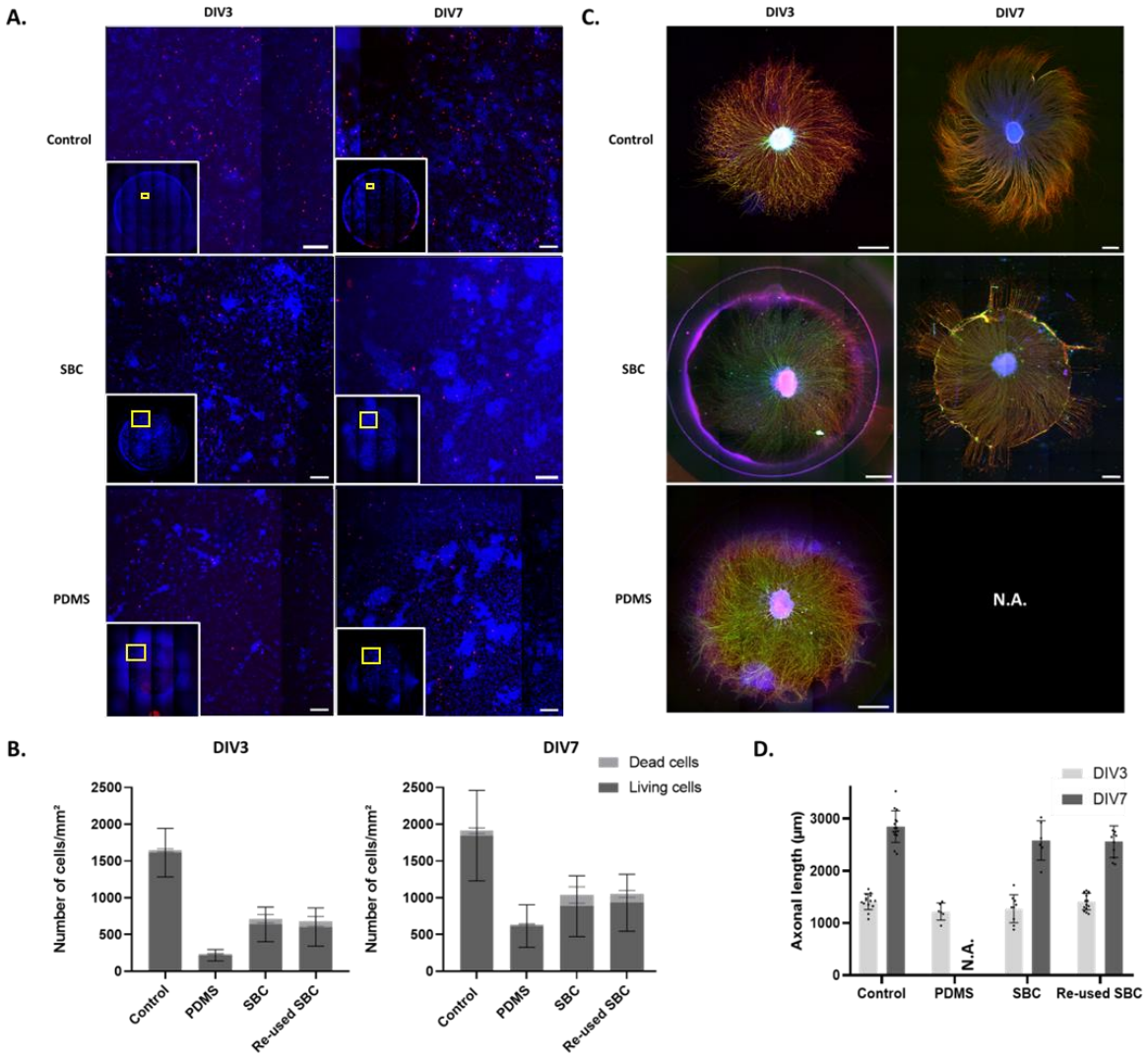

Figure 3: Comparison of viability and axonal growth within the chips A. Tiles of a control well and a central chamber of a SBC and a PDMS chip at DIV3 and DIV7. The images show all cells (blue) and dead cells (green). Scale bars = 50 µm **B.** The number of living and dead cells per mm² inside the controls, PDMS chips, SBC chips and reused SBC chips at DIV3 and DIV7. DRG n=6-24, embryos e=6-12. Results are represented as the mean±SEM. Two-way ANOVA were performed. The alpha value threshold was set at 5% and the *P*-values are represented as follows: *p< 0.05, **p< 0.01, ***p< 0.001. **C.** Tiles of DRG explants inside the controls, PDMS chips, SBC chips and reused SBC chips at DIV3 and DIV7. Nuclei (blue), neurofilaments H (green), SMI312 (red). Scale bars = 500 µm **D.** Axonal length inside the controls, PDMS chips, SBC chips and reused SBC chips at DIV3 and DIV7. No data is available for PDMS chips at DIV7, as it was not possible to measure the axonal length. n=6-15, e=6-12. Results are represented as the mean±SEM. Two- way ANOVA tests were conducted. The alpha value threshold was set at 5% and the *P*-values are represented as follows: *p< 0.05, **p< 0.01, ***p< 0.001. *P*-values are represented for the living cells

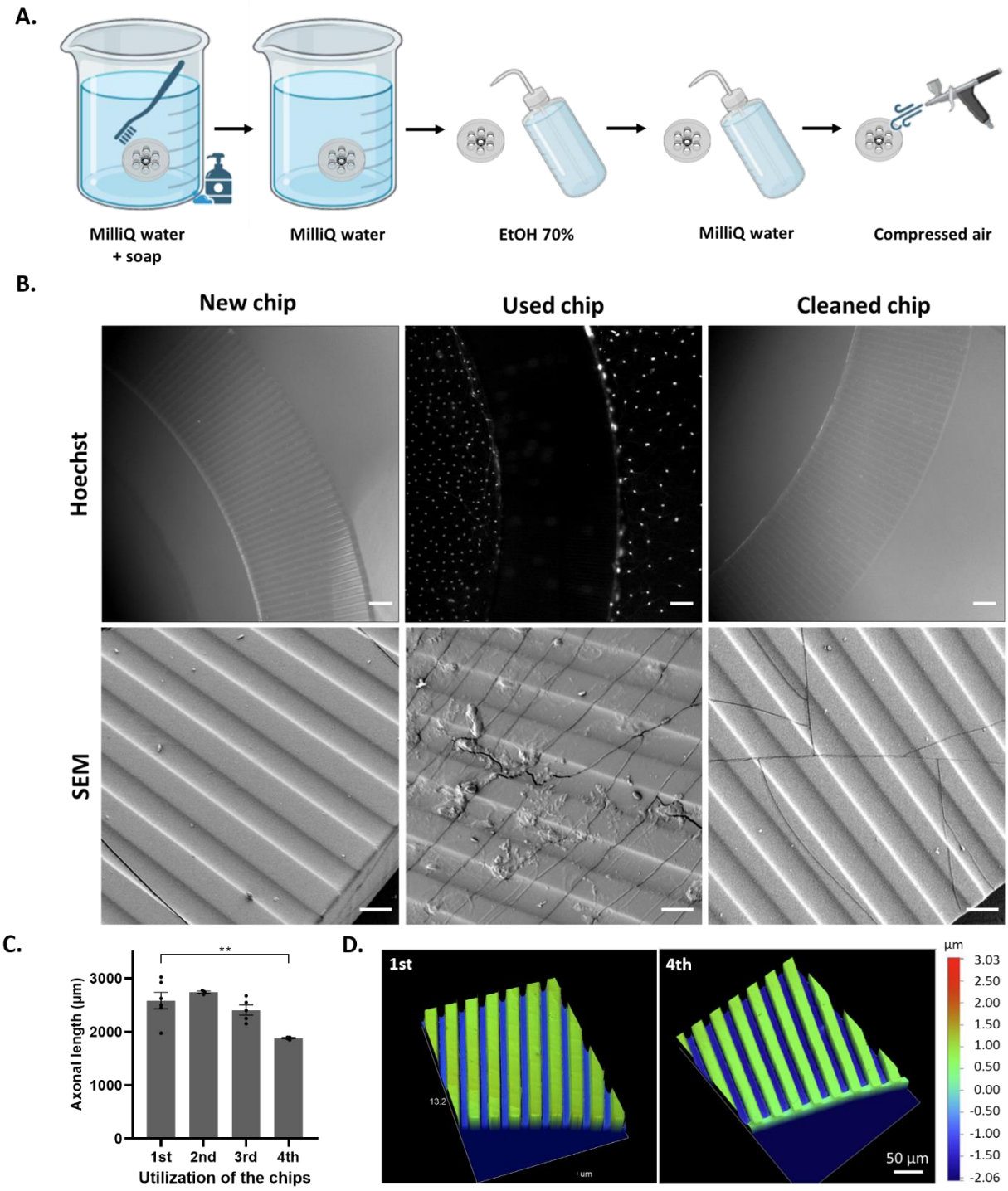

Figure 4: Reusability of SBC chips A. Cleaning process of the two-layer microfluidic chip in SBC. **B.** Hoechst staining (scale bar = 100 µm) and SEM (scale bar = 10 µm) imaging on a new, a used and a cleaned SBC chip. **C.** Axonal length of DRGs at DIV7 depending on the number of uses of the SBC chip. DRG n=3-6, embryos e=3-6. The results are presented as the mean±SEM. A Tukey's multiple comparison test was conducted. The alpha value threshold was set at 5%, and the *P*-values are represented as follows: *$p < 0.05$, **$p < 0.01$, ***$p < 0.001$. **D.** Optical profilometry of the microchannels of a new SBC chip and a SBC chip used four times.

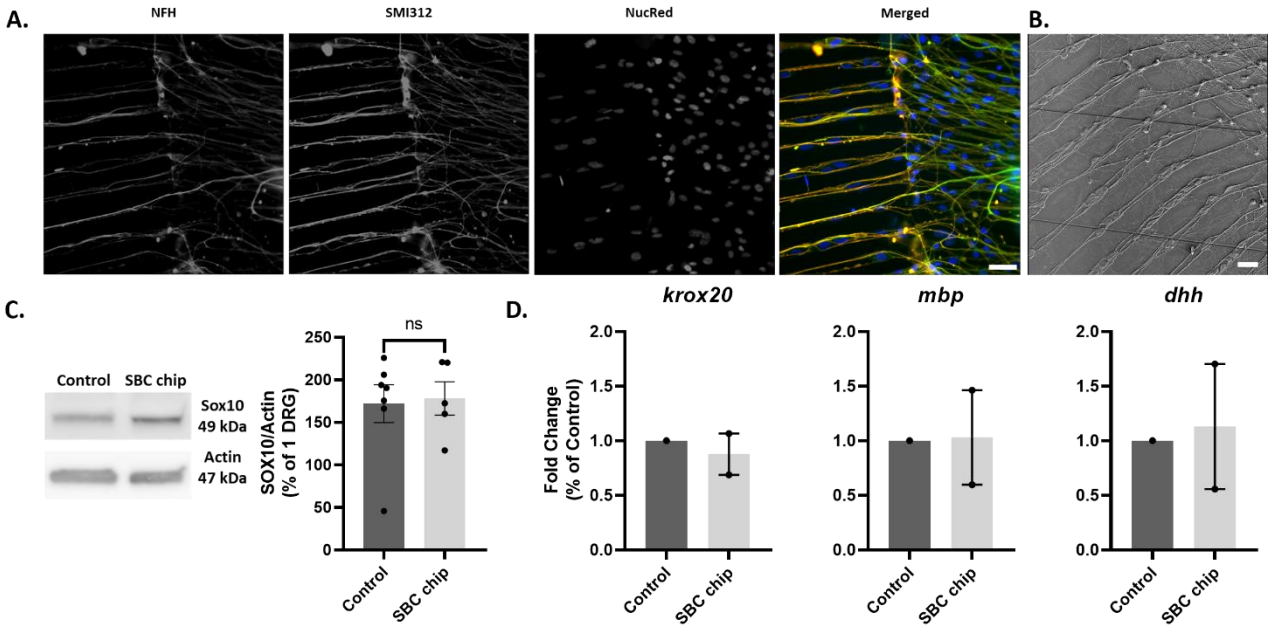

Figure 5: Direct accessibility to cells A. Immunostaining of the neurofilaments of a DRG at DIV7 after opening of the chip. Nuclei (blue), neurofilaments H (green), SMI312 (red). **B.** SEM image of the neurofilaments of a DRG at DIV21. Scale bars represent 20 µm **C.** Western blot analysis of 4 explants DRGs at DIV11 in controls and in SBC opened chips and corresponding graph representing Sox10 expression. Actin was used as a loading control. Results represent the mean ± SEM of three independent experiments (n=5-8, embryo e=3). A t-test was performed for statistical analysis (ns=non-significant). **D.** RT-qPCR analysis of *Krox20*, *Mbp* and *Dhh* genes of one DRG at DIV7 in controls and in SBC chips. Results represent the mean ± SEM of three independent experiments (n=6-10, embryo e≥5). A Mann-Whitney-test was performed for statistical analysis (ns=non-significant).

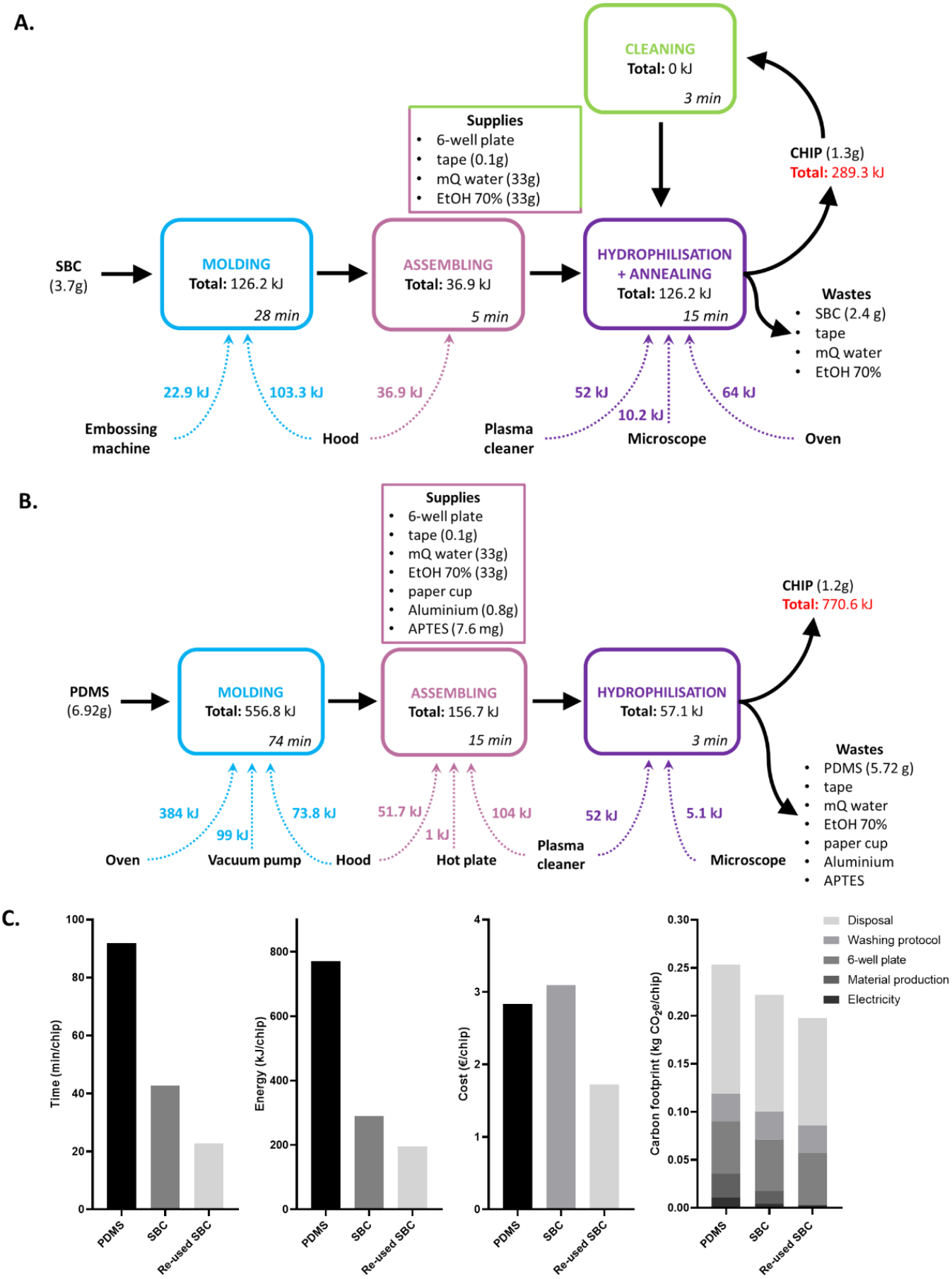

Figure 6: Assessment of the resources used and CO2 emissions generated to produce a SBC and a PDMS device.

Energy consumption of the different steps of a fabrication process for **A.** a SBC-based chip and **B.** PDMS-based chip. **C.** Comparison of the time, energy, cost and carbon footprint associated to the fabrication of a PDMS, a SBC and a reused SBC chip.